



Mechanisms of Future Predicted Changes in the Zonal Mean Mid-Latitude Circulation

Tiffany A. Shaw¹

Published online: 21 November 2019
© The Author(s) 2019

Abstract

State-of-the-art climate models predict the zonal mean mid-latitude circulation will undergo a poleward shift and seasonally and hemispherically dependent intensity changes in the future. Here I review the mechanisms put forward to explain the zonal mean mid-latitude circulation response to increased carbon dioxide (CO₂) concentration. The mechanisms are grouped according to their thermodynamic starting point, which are thought to arise from processes independent of the zonal mean mid-latitude circulation response. There are 24 mechanisms and 8 thermodynamic starting points: (i) increased latent heat release aloft in the tropics, (ii) increased dry static stability and tropopause height outside the tropics, (iii) radiative cooling of the stratosphere, (iv) Hadley cell expansion, (v) increased specific humidity following the Clausius-Clapeyron relation, (vi) cloud radiative effect changes, (vii) turbulent surface heat flux changes, and (viii) decreased surface meridional temperature gradient. I argue progress can be made by testing the thermodynamic starting points. I review recent tests of the increased latent heat release aloft in the tropics starting point, i.e., prescribing diabatic perturbations, quantifying the transient response to an abrupt CO₂ increase and imposing latitudinally dependent CO₂ concentration. Finally, I provide a future outlook for improving our understanding of predicted changes in the zonal mean mid-latitude circulation.

Keywords Circulation · Climate change

Introduction

The zonal mean mid-latitude circulation on Earth encompasses surface westerlies, upper level jet streams, storm tracks, eddies or Rossby waves, and the Ferrel circulation. Decades of research has established that the midlatitudes is an eddy-dominated regime. More specifically, eddies dominate (1) the surface westerlies via eddy momentum flux convergence [50], (2) the thermally indirect Ferrel circulation via eddy heat fluxes [28, 48], and (3) the transport of moist static energy (MSE, i.e., the sum of dry static and latent energy) between the equator and the pole [62].

For over four decades state-of-the-art climate models have predicted zonal mean mid-latitude circulation changes

in response to increased greenhouse gas (GHG) concentrations, primarily increased carbon dioxide (CO₂) concentration. The earliest prediction comes from Manabe and Wetherald [37] who showed zonal mean eddy kinetic energy (EKE) in the upper troposphere shifts poleward in response to a doubling of CO₂ (see their Fig. 11). Hall et al. [18] showed a poleward shift also occurs for other storm track metrics, including low-level eddy temperature and moisture fluxes. The poleward shift of the zonal mean storm tracks has been reproduced in more recent climate model intercomparisons and is largest in the Southern Hemisphere (SH) [1, 2, 8]. In addition, storm track intensity increases in response to increased CO₂ in the SH [47]. However, in the Northern Hemisphere (NH), the intensity changes are seasonally dependent: intensity increases during winter but decreases during summer [47].

The zonal mean storm track response to increased CO₂ coincides with a poleward shift of the zonal mean mid-latitude westerlies and eddy momentum flux convergence maximum, and a strengthening of the eddy-driven jet [1, 56]. The poleward shift is largest in the SH and is robust across the seasonal cycle [56]. Overall, the storm track and eddy-driven jet changes in the SH are more robust

This article is part of the Topical Collection on *Mid-latitude Processes and Climate Change*

✉ Tiffany A. Shaw
tas1@uchicago.edu

¹ Department of the Geophysical Sciences, The University of Chicago, 5734 South Ellis Ave., Chicago, IL, 60637, USA

than those in the NH because of the presence of opposing thermodynamic influences in the NH [20, 51], e.g., the meridional temperature gradient response at the surface and in the upper troposphere are opposite (Fig. 1, top). Thus, the emergent robust multi-model mean response of the zonal mean mid-latitude circulation to increased CO₂ includes (1) a poleward shift, (2) an intensity increase in the SH and during NH winter, and (3) an intensity decrease during NH summer.

The predicted zonal mean mid-latitude circulation response is important because it is connected to changes in the hydrological cycle, individual storms, and extreme events [51]. To date, there is some observational evidence for the poleward shift of the zonal mean mid-latitude circulation [3, 15] and the weakening of the NH storm

track during summer [12]. However, in the SH, the observed poleward shift during SH summer most likely reflects the circulation response to ozone depletion [30].

Simulation does not equal understanding [21]. Confidence in the emergent zonal mean mid-latitude circulation response to increased CO₂ predicted by state-of-the-art climate models requires a physically based explanation of the underlying mechanisms. Physically based explanations can be achieved using analytical models (equations), scaling arguments, or a hierarchy of numerical models of varying physical complexity. A success of climate theory has been the physically based explanation of several emergent zonal mean thermodynamic responses to increased CO₂ predicted by state-of-the-art climate models (Fig. 1, top), e.g., amplified warming aloft in the tropics, amplified warming at the surface in the Arctic, rising of the tropopause [13, 20, 64], and the wet-get-wetter and dry-get-drier response of the hydrological cycle [22]. Unfortunately, similar success does not exist for the response of the zonal mean mid-latitude circulation to increased CO₂ (Fig. 1, bottom). Instead, multiple mechanisms have been proposed, which have not been sufficiently tested.

Here I review the mechanisms that have been proposed to explain the predicted zonal mean mid-latitude circulation response to increased CO₂. There are many possible ways to define and organize the mechanisms. I choose to define a mechanism broadly, i.e., I include all idealized modeling results that demonstrate a mid-latitude circulation response by changing some factor even if the detailed chain of causality is not clear. I choose to organize the mechanisms according to their thermodynamic starting point, which are thought to arise from processes independent of the zonal mean mid-latitude circulation response, e.g., tropical convective adjustment or stratospheric radiative adjustment. Before reviewing the mechanisms, I briefly review some relevant frameworks. I then review the mechanisms proposed to explain the (1) poleward shift, (2) intensity increase, and (3) intensity decrease response of the zonal mean mid-latitude circulation to increased CO₂. I argue progress can be made by testing the thermodynamic starting points. I review recent tests of the thermodynamic starting point tied to tropical convective adjustment. Finally, I provide a future outlook for understanding the zonal mean mid-latitude circulation response to increased CO₂.

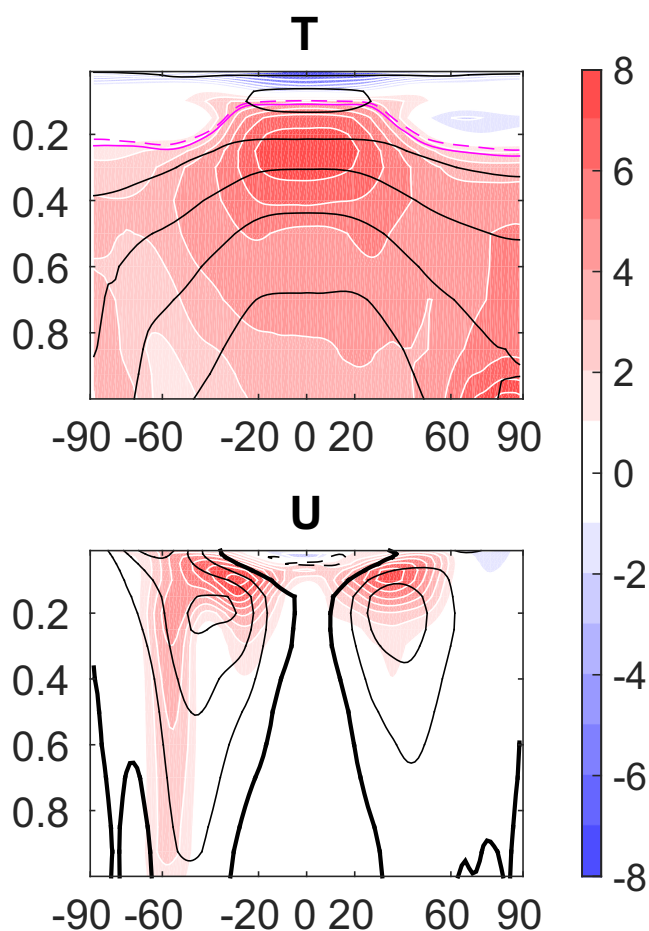


Fig. 1 Response of annual and zonal mean temperature (top, shading, contour interval 1 K) and zonal wind (bottom, shading, contour interval 1 ms⁻¹) from the CMIP5 ECHAM6 (MPI-ESM-LR, 58) RCP8.5 (2080–2099) minus historical (1986–2005) simulations. Climatology indicated by black contours; contour interval 20 K up to 300 K for temperature and contour interval 10 ms⁻¹ for zonal wind. WMO tropopause for the climatology and increased CO₂ climate indicated by solid and dashed magenta lines, respectively

Background on Relevant Frameworks

Before reviewing the mechanisms that have been proposed to explain the zonal mean mid-latitude circulation response to increased CO₂, it is useful to review some relevant dynamical frameworks.

Barotropic Rossby Wave Dynamics

Assuming eddies can be usefully described as plane waves with perturbation streamfunction $\psi' = Re[A \exp i(kx + \ell y - \omega t)]$ where A is the wave amplitude, k is the zonal wavenumber, ℓ is the meridional wavenumber, and ω is the frequency then they are governed by the Rossby wave dispersion relation:

$$\omega = \bar{u}k - \frac{\beta^*k}{k^2 + \ell^2} \tag{1}$$

or

$$c = \bar{u} - \frac{\beta^*}{k^2 + \ell^2} \tag{2}$$

where c is the eddy phase speed, \bar{u} is the background zonal mean zonal wind, $\beta^* = \beta - \partial^2\bar{u}/\partial y^2$ is the meridional gradient of the absolute vorticity, and

$$\ell = \pm \left(\frac{\beta^*}{\bar{u} - c} - k^2 \right)^{1/2} \tag{3}$$

[63]. The sign convention of the meridional wave number is such that poleward propagation ($\ell > 0$ in NH and $\ell < 0$ in SH) occurs poleward of the wave source (poleward side of the jet) and equatorward propagation ($\ell < 0$ in NH and $\ell > 0$ in SH) occurs equatorward of the wave source (equatorward side of the jet). Linear theory predicts eddies propagate away from their source region and dissipate (break) at the critical latitude where $\bar{u} = c$ ($\ell \rightarrow \infty$) or reflect at the turning latitude where $\ell = 0$.

An equation for the eddy momentum flux can be derived using the relationship between the velocity components and the stream function, i.e., $v' = \partial\psi'/\partial x$ and $u' = -\partial\psi'/\partial y$:

$$\overline{u'v'} = -\frac{1}{2}A^2k\ell = \mp\frac{1}{2}A^2k \left(\frac{\beta^*}{\bar{u} - c} - k^2 \right)^{1/2} \tag{4}$$

Consistent with the sign convention discussed above, poleward of the source the eddy momentum flux is equatorward ($\overline{u'v'} < 0$ in NH and $\overline{u'v'} > 0$ in SH) and equatorward of the source the eddy momentum flux is poleward ($\overline{u'v'} > 0$ in the NH and $\overline{u'v'} < 0$ in the SH). Thus, eddies propagate away from the source region converging momentum flux into that region and drive surface westerlies [50], i.e., $\overline{\tau_u} \approx -\partial(\langle u'v' \rangle)/\partial y > 0$ where τ_u is the zonal surface wind stress and $\langle \cdot \rangle$ is a mass-weighted vertical integral. Hereafter, the eddy-driven jet is referred to as the jet.

Simpson et al. [56] showed that the response of the zonal mean mid-latitude westerlies to increased CO₂ is dominated by eddy momentum flux convergence changes, i.e.,

$$\Delta\overline{\tau_u} \approx -\partial(\langle \Delta u'v' \rangle)/\partial y. \tag{5}$$

According to barotropic dynamics, a change in eddy momentum flux can be decomposed as follows:

$$\Delta\overline{u'v'} \approx -Ak\ell\Delta A - \frac{1}{2}A^2(\ell\Delta k + k\Delta\ell) \tag{6}$$

where

$$\Delta\ell = \frac{1}{2\ell} \frac{\Delta\beta^*}{(\bar{u} - c)} - \frac{\beta^*}{2\ell} \frac{\Delta(\bar{u} - c)}{(\bar{u} - c)^2} - \frac{k}{\ell} \Delta k \tag{7}$$

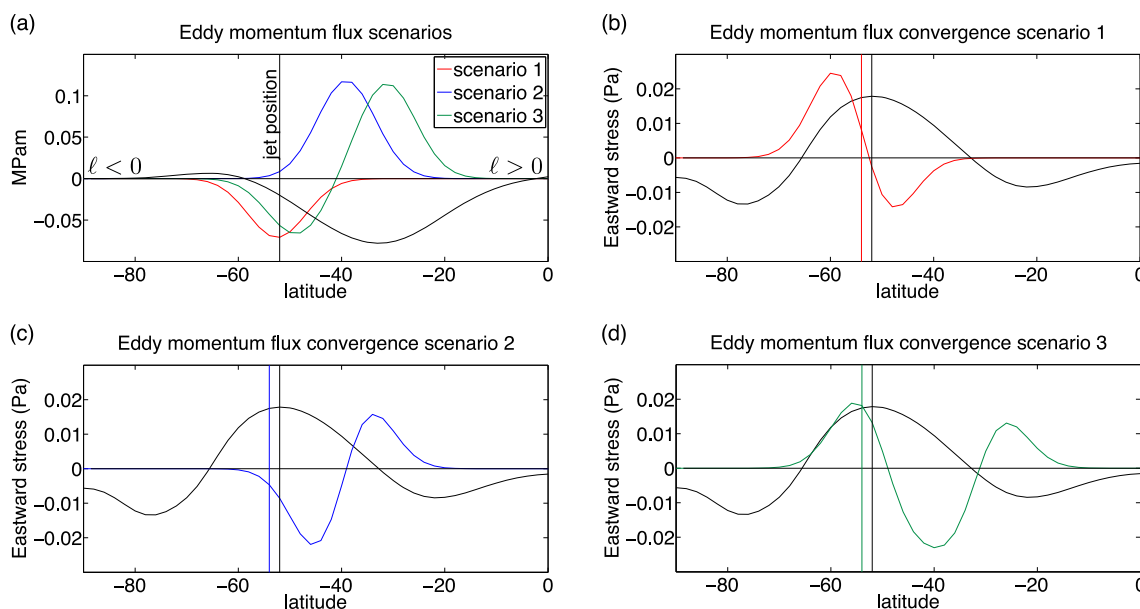


Fig. 2 Schematic of possible scenarios of **a** vertically integrated eddy momentum flux ($\langle u'v' \rangle$) and **b–d** vertically integrated eddy momentum flux convergence ($-\partial_y \langle u'v' \rangle$) responses to increased CO₂ relative to climatology (black, divided by 10) in the SH. Vertical colored lines

in **b–d** indicate the position of maximum eddy momentum flux convergence for the different scenarios relative to the climatology (vertical black line). See text for more discussion

and

$$\Delta\beta^* = -\frac{\partial^2 \Delta\bar{u}}{\partial y^2}. \quad (8)$$

Three possible scenarios of the eddy momentum flux response to increased CO₂ that lead to a poleward shift of the eddy momentum flux convergence maximum, i.e., the surface westerlies, are illustrated schematically in Fig. 2. Since the meridional wave number and wave propagation are hemisphere dependent, we illustrate the scenarios for the SH. In the first scenario, there is increased poleward momentum flux (equatorward wave propagation, Fig. 2a, red line) around the jet position (Fig. 2a, vertical black line), which leads to a dipole response of the eddy momentum flux convergence (Fig. 2b, red line) that shifts the jet poleward (Fig. 2b, vertical red line). In the second scenario, there is increased equatorward momentum flux (poleward wave propagation, Fig. 2a, blue line) equatorward of the jet position, which decreases the eddy momentum flux convergence on the equatorward side (Fig. 2c, blue line) and shifts the jet poleward (Fig. 2c, vertical blue line). Finally, in the third scenario, there is an eddy momentum flux dipole (Fig. 2a, green line), which shifts the latitude of maximum value of the eddy momentum flux poleward. This leads to a tripole response of the eddy momentum flux convergence (Fig. 2d, green line) that shifts the jet poleward (Fig. 2d, vertical green line). Clearly, there are multiple ways barotropic dynamics can explain a poleward jet shift as discussed in more detail in the section “Mechanisms Explaining the Poleward Shift of the Zonal Mean Mid-Latitude Circulation” below.

Baroclinic Rossby Wave Dynamics

Assuming eddies can be usefully described as plane waves in the zonal direction then their meridional and vertical structure is determined by solving the quasi-geostrophic potential vorticity (PV) equation (a wave equation), which includes a mean-state quasi-geostrophic index of refraction, i.e.,

$$n^2 = \left[\frac{\partial \bar{P}/\partial y}{a(\bar{u} - c)} - \left(\frac{k}{a \cos \phi} \right)^2 - \left(\frac{f}{2NH} \right)^2 \right] a^2 \quad (9)$$

where \bar{P} is the time and zonal mean PV, f is the Coriolis parameter, N is the buoyancy frequency, and H is the density-scale height [38]. Assuming WKB conditions and linearity, Rossby waves are refracted by gradients of n^2 : they propagate toward regions of large n^2 [24]. Thus, a change in the index of refraction affects wave propagation and is often dominated by changes in the mean PV gradient

and eddy phase speed, i.e.,

$$\Delta n^2 \approx \frac{\partial \Delta \bar{P}/\partial y}{(\bar{u} - c)/a} - \frac{\partial \bar{P}/\partial y}{(\bar{u} - c)^2/a} \Delta c. \quad (10)$$

Potential Vorticity Dynamics

The steady-state response of the zonal mean mid-latitude westerlies can be connected to the response of the eddy PV flux ($\overline{v'P'}$) and the thermal forcing (Q) following [36]:

$$\frac{\partial^2}{\partial y^2} \Delta \bar{F} = -\frac{\partial^2}{\partial y^2} (\Delta \overline{v'P'}) + \frac{\partial^2}{\partial y^2} \left(\frac{f \Delta \bar{Q}}{\partial \theta / \partial z} \right) \quad (11)$$

where F is the frictional damping of the zonal mean zonal wind and θ is potential temperature. If the eddy PV flux is assumed to be down-gradient, then a change in the eddy PV flux can be decomposed as follows:

$$\Delta \overline{v'P'} \approx -\Delta K_{\text{eff}} \frac{\partial \bar{P}}{\partial y} - K_{\text{eff}} \frac{\partial \Delta \bar{P}}{\partial y} \quad (12)$$

where K_{eff} is the effective diffusivity, which can be quantified using the finite amplitude wave activity budget [44, 45].

Mean Available Potential Energy

According to the Lorenz energy cycle, EKE is driven by Mean Available Potential Energy (MAPE). MAPE scales linearly with EKE in idealized simulations and reanalysis data [40, 46, 47]. O’Gorman and Schneider [46] derived the following scaling estimate for MAPE:

$$\text{MAPE} \approx \frac{c_p p_0}{24g} (\sigma_s - \sigma_t^{\text{max}}) L_Z^2 [\Gamma]_v [\{\partial_y \bar{T}\}]_v^2 \quad (13)$$

where $\{\cdot\}$ is an average over the baroclinic zone, $[\cdot]_v$ is a vertical average over model sigma levels from σ_t^{max} (model top) to $\sigma_s = 0.9$, L_Z is the width of the baroclinic zone, $\Gamma = -\kappa \{\partial \bar{\theta} / \partial p\}^{-1} / \{\bar{p}\}$ is an inverse measure of the dry static stability, and the other symbols have their usual meaning. MAPE is proportional to the square of the Eady growth rate. Changes in MAPE affect the storm track position and intensity and are typically dominated by changes in the inverse dry static stability and meridional temperature gradient, i.e.,

$$\begin{aligned} \Delta \text{MAPE} &\approx \frac{c_p p_0}{24g} (\sigma_s - \sigma_t^{\text{max}}) \\ &L_Z^2 \left(\Delta [\Gamma]_v [\{\partial_y \bar{T}\}]_v^2 + [\Gamma]_v \Delta [\{\partial_y \bar{T}\}]_v^2 \right). \end{aligned} \quad (14)$$

Energy Budget

The dominant components of eddy energy transport are dry static and latent energy, which combine to form MSE. Since

the eddy energy flux maximizes in the lower troposphere and is down-gradient [29], it is often closed diffusively, i.e.,

$$\langle \overline{v'm'} \rangle = -D_m \frac{\partial \overline{m}}{\partial y} \tag{15}$$

$$\langle \overline{v's'} \rangle = -D_s \frac{\partial \overline{s}}{\partial y} \approx -c_p D_s \frac{\partial \overline{T}}{\partial y} \tag{16}$$

where $\langle \cdot \rangle$ denotes a mass-weighted vertical integration, $m = c_p T + gZ + L_v q$ is the MSE, $s = c_p T + gZ$ is the dry static energy (DSE). The mean meridional gradient ($\partial \overline{m}/\partial y$, $\partial \overline{s}/\partial y$ or $\partial \overline{T}/\partial y$) is taken to be near the surface consistent with energy balance models (EBMs). A change in the eddy energy flux can be decomposed as follows:

$$\Delta \langle \overline{v'm'} \rangle = -\Delta D_m \frac{\partial \overline{m}}{\partial y} - D_m \frac{\partial \Delta \overline{m}}{\partial y} \tag{17}$$

$$\Delta \langle \overline{v's'} \rangle = -\Delta D_s \frac{\partial \overline{s}}{\partial y} - D_s \frac{\partial \Delta \overline{s}}{\partial y}. \tag{18}$$

Held and Soden [22] showed the latent energy flux ($\langle \overline{Lv'q'} \rangle$) in mid-latitudes increases following the Clausius-Clapeyron relation in response to increased CO₂ in coupled climate models, i.e., $\Delta \langle \overline{Lv'q'} \rangle \approx \alpha \Delta T \langle \overline{Lv'q'} \rangle$ where ΔT is the change in global mean surface temperature and $\alpha \approx 7\%/K$.

Recently, Barpanda and Shaw [2] and Shaw et al. [53] derived a MSE framework that connects changes in storm track position and intensity to (1) changes in energy input to the atmosphere (shortwave absorption, surface heat fluxes and outgoing longwave radiation or OLR) and (2) changes in the MSE flux by the stationary circulation (mean meridional circulation and stationary eddies). More specifically, a change in storm track intensity can be written as follows:

$$\Delta \langle \overline{v'm'} \rangle |_{\phi_s} = 2\pi a^2 \int_{\phi_s}^{-\pi/2} \cos \phi (\Delta F_{SWABS} + \Delta F_{SHF} - \Delta F_{OLR}) d\phi - 2\pi a \cos \phi_s \Delta \langle \overline{v} \overline{m} \rangle |_{\phi_s} \tag{19}$$

where ϕ_s is the storm track position (latitude of maximum value of the eddy MSE flux), ΔF_{SWABS} , ΔF_{SHF} , and ΔF_{OLR} are the change in shortwave absorption, surface heat fluxes and OLR respectively, and $\Delta \langle \overline{v} \overline{m} \rangle$ is the change in the MSE flux by the stationary circulation.

Mechanisms Explaining the Poleward Shift of the Zonal Mean Mid-Latitude Circulation

Here I review the mechanisms that have been proposed to explain the poleward shift of the zonal mean mid-latitude circulation in response to increased CO₂. The

mechanisms are grouped according to their thermodynamic starting point.

Increased Latent Heat Release Aloft in the Tropics

Increased CO₂ increases latent heat release aloft in the tropics due to warmer and moister surface air parcels and assuming moist adiabatic adjustment [20, 64]. The enhanced latent heat release aloft increases the dry static stability of the tropics and strengthens the subtropical meridional temperature gradient in the upper troposphere, which accelerates the subtropical jet via thermal wind balance. The following mechanisms are connected to increased tropical latent heat release aloft:

- Butler et al. [4] showed a prescribed diabatic heating in the tropical upper troposphere shifts the storm track and jet poleward in dry dynamical core simulations. Butler et al. [5] argued the prescribed diabatic heating results in a poleward shift of the mean PV gradient, which enhances the eddy PV flux, i.e., $\Delta v'P' \approx -K_{\text{eff}} \partial \Delta \overline{P} / \partial y$ assuming $\Delta K_{\text{eff}} \approx 0$ (see Eq. 12), on the poleward side of the jet shifting the eddies and circulation poleward. Figure 8 in [5] is a schematic of their mechanism.
- Riviere [49] showed that when the meridional temperature gradient in the upper troposphere is increased in a three-level quasi-geostrophic model, long waves become more unstable, and the increased eddy length scale favors anticyclonic wave breaking and a poleward shift of the jet.
- Kidston and Vallis [27] and Lorenz [33] used barotropic models to show that the acceleration of the zonal wind aloft reduces the meridional gradient of the absolute vorticity on the flanks of the jet ($\Delta \beta^* = -\partial^2 \Delta \overline{u} / \partial y^2 < 0$, see Eq. 8), which affects the turning latitude (where $\ell = 0$) on the poleward side of the jet. There is increased wave reflection from the poleward side of the jet, equatorward wave propagation ($\Delta \ell \approx \Delta \beta^* / 2\ell(\overline{u} - c) > 0$ in the SH, see Eq. 7), a poleward momentum flux response ($\Delta \overline{u'v'} \approx -A^2 k \Delta \ell / 2 < 0$ in the SH, see Eq. 6), and a poleward shift of the jet. This is analogous to scenario 1 in Fig. 2.
- Lu et al. [36] showed that the eddy PV flux response to prescribed diabatic heating in the tropical upper troposphere in a dry dynamical core model leads to a poleward shift of the jet due to a change in effective diffusivity ($\Delta v'P' \approx -\Delta K_{\text{eff}} \partial \overline{P} / \partial y$, see Eq. 12) rather than due to a change in the mean PV gradient, which was argued to be the important factor by [5] (see above). Their results were based on the finite amplitude wave activity budget. Figure 10 in [36] is a schematic of their mechanism.

Increased Dry Static Stability and Tropopause Height Outside the Tropics

Increased CO₂ increases the dry static stability and tropopause height outside the tropics in state-of-the-art climate models [64]. While the cause of the stability and tropopause height responses may not be independent of the circulation response, the following mechanisms rely on vertical temperature changes outside the tropics:

- Lorenz and DeWeaver [32] showed that artificially raising the tropopause poleward of the climatological jet shifts the jet poleward in dry dynamical core simulations. Interestingly, raising the tropopause equatorward of the climatological jet shifts the jet equatorward.
- Frierson [14] argued increased subtropical dry static stability reduces eddy generation on the equatorward side of the jet ($\Delta A < 0$ where $\ell > 0$ in the SH), leading to an equatorward momentum flux response ($\Delta \overline{u'v'} \approx -Ak\ell\Delta A > 0$ in the SH, see Eq. 6) and a poleward jet shift. This is analogous to scenario 2 in Fig. 2.
- Chen et al. [10] and Lu et al. [35] argued that the increased extratropical tropopause height increases the meridional temperature gradient and zonal wind, and leads to faster eddy phase speeds ($\Delta(\overline{u} - c) < 0$), a poleward shift of the critical latitude (where $\overline{u} = c$) on the equatorward side of the jet, equatorward wave propagation ($\Delta\ell \approx -\beta^* \Delta(\overline{u} - c)/(2\ell(\overline{u} - c)^2 > 0$ in the SH, see Eq. 7), a poleward shift of the latitude of maximum absolute value of the eddy momentum flux, and a poleward shift of the jet. This is analogous to scenario 3 in Fig. 2.
- Kidston et al. [25, 26] argued that increased dry static stability causes an increase in the eddy length scale, i.e., Rossby radius of deformation $L_R = NH/f$, thus $\Delta k < 0$, a decrease in the eddy phase speed relative to the background mean wind, a poleward shift of the critical line (where $\overline{u} = c$) on the poleward side of the jet, a poleward momentum flux response ($\Delta \overline{u'v'} \approx -A\ell\Delta k < 0$ in the SH, see Eq. 6), leading eddies to dissipate further poleward, and shifting the jet poleward. This is analogous to scenario 1 in Fig. 2.

Radiative Cooling of the Stratosphere

Increased CO₂ cools the stratosphere via radiative adjustment [20, 64]. The following mechanisms rely on the stratospheric response:

- Sigmund et al. [55] showed that doubling CO₂ only in the middle atmosphere (above the climatological tropopause) shifts the jet poleward in a prescribed

sea surface temperature (SST) atmospheric general circulation model (AGCM).

- Butler et al. [4] showed that a prescribed diabatic cooling in the polar lower stratosphere shifts the storm track and jet poleward in dry dynamical core simulations.
- Wu et al. [68] showed that the transient evolution of the poleward shift of the jet in response to CO₂ doubling in an AGCM was dominated by changes in the stratosphere. More specifically, the subpolar lower stratospheric zonal wind response increased the index of refraction via the mean PV gradient ($\Delta n^2 \approx (\partial \Delta \overline{P}/\partial y)/(\overline{u} - c)/a > 0$, see Eq. 9) on the poleward side of the jet such that eddies propagate further poleward and shift the jet poleward.

Hadley Cell Expansion

Increased CO₂ leads to a poleward shift of the Hadley cell edge [34], and several theories have been proposed to explain its poleward shift [57]. Mbengue and Schneider [39, 40] showed the Hadley cell and storm track shifts were related in dry dynamical core simulations via MAPE changes that were dominated by the meridional temperature gradient response ($\Delta \text{MAPE} \approx \frac{c_p p_0}{24g} (\sigma_s - \sigma_t^{\max}) L_Z^2 [\Gamma]_v \Delta[\{\partial_y \overline{T}\}]_v^2$, see Eq. 14). Mbengue and Schneider [41] showed the expansion of the Hadley cell shifts the near-surface meridional temperature gradient poleward, which shifts the latitude of maximum MAPE, and thus the storm track poleward in an EBM. An equation linking the storm track position to the Hadley cell edge and near-surface meridional temperature gradient can be derived using the EBM (see equation 10 in [41]).

Increased Specific Humidity Following the Clausius-Clapeyron Relation

Increased CO₂ increases the saturation specific humidity and near-surface specific humidity following the Clausius-Clapeyron relation [22]. The following mechanisms rely on changes in specific humidity following the Clausius-Clapeyron relation:

- Held [23] argued that if the total MSE flux is constant in response to increased CO₂ ($\Delta \langle v'm' \rangle = \Delta \langle Lv'q' \rangle + \Delta \langle v's' \rangle \approx 0$), then increased latent energy flux following the Clausius-Clapeyron relation ($\Delta \langle Lv'q' \rangle \approx \alpha \Delta T \langle Lv'q' \rangle < 0$ in the SH) should result in decreased DSE flux ($\Delta \langle v's' \rangle > 0$ in the SH). Since the increased latent energy flux occurs on the equatorward side of the latitude of the maximum absolute value of the DSE flux, the corresponding DSE flux decrease leads to a poleward shift of the latitude of maximum absolute

value of the DSE flux, i.e., a poleward shift of the dry storm track.

- Shaw and Voigt [52] showed that if the total MSE flux is constant in response to SST warming ($\Delta\langle v'm' \rangle \approx 0$) and the near-surface meridional MSE gradient response to increased CO₂ follows the Clausius-Clapeyron relation ($\partial\Delta\bar{m}/\partial y \approx \alpha^2\Delta TLq\partial\bar{T}/\partial\phi/a$), then the eddy diffusivity change [$\Delta D_m \approx -D_m(\alpha^2\Delta TLq\partial\bar{T}/\partial\phi/a)/(\partial\bar{m}/\partial y)$], see Eq. 17 with $\Delta\langle v'm' \rangle \approx 0$ and $\partial\Delta\bar{m}/\partial y \approx \alpha^2\Delta TLq\partial\bar{T}/\partial\phi/a$] shifts the maximum diffusivity, i.e., the storm track, poleward in aquaplanet models.

Cloud Radiative Effect Changes

Increased CO₂ leads to an upward shift of high clouds, which impacts the longwave cloud radiative effect (CRE). There is also an increase in cloud-liquid water in mid-to-high latitudes in response to warming, which primarily impacts the shortwave CRE [6]. While it is unclear how much of the CRE response to increased CO₂ is shaped by the circulation, the following mechanisms rely on CRE changes.

- Voigt and Shaw [65] showed that prescribing the cloud radiative response to warming in climatological prescribed SST aquaplanet simulations leads to a poleward jet shift. Voigt and Shaw [66] showed the poleward shift is dominated by the response of mid-latitude (20–50°) high clouds.
- Shaw and Voigt [52] showed the atmospheric CRE (ACRE) response (top of atmosphere minus surface CRE) to warming in prescribed SST aquaplanet simulations implies a change in atmospheric energy transport ($\Delta\langle \bar{v}\bar{m} \rangle = 2\pi a^2 \int_{-\pi/2}^{\phi} \cos\phi \Delta F_{ACRE} d\phi$) that shifts the latitude of the maximum absolute value of the MSE transport poleward.
- Ceppi and Hartmann [7] showed that prescribing the shortwave cloud radiative response to increased CO₂ in a climatological slab-ocean aquaplanet simulation dominates the poleward shift of the mid-latitude circulation.
- Li et al. [31] showed that prescribing the high-cloud radiative response in a dry dynamical core shifts the jet poleward.

Mechanisms Explaining the Intensification of the Zonal Mean Mid-Latitude Circulation

Here I review the mechanisms that have been proposed to explain the intensification of the zonal mean mid-latitude circulation in response to increased CO₂. Once again, the mechanisms are grouped according to their thermodynamic starting point.

Increased Latent Heat Release Aloft in the Tropics

- Held [20] argued that an increase in the meridional temperature gradient aloft should increase eddy energy ($\Delta A > 0$), leading to an equatorward momentum flux response poleward of the source ($\Delta\langle u'v' \rangle \approx -Ak\ell\Delta A > 0$ where $\ell < 0$ in the SH, see Eq. 6), a poleward momentum flux response equatorward of the source ($\Delta\langle u'v' \rangle \approx -Ak\ell\Delta A < 0$ where $\ell > 0$ in the SH, see Eq. 6), convergence of eddy momentum flux into the source region and a strengthening of the jet.
- O’Gorman [47] showed the EKE increase in response to increased CO₂ in the SH and during NH winter follows an increase in MAPE. The MAPE increase in the SH was connected to the robust increase of the meridional temperature gradient in the upper troposphere ($\Delta\text{MAPE} \approx \frac{c_p p_0}{24g} (\sigma_s - \sigma_t^{\max}) L_Z^2 [\Gamma]_v \Delta\{\partial_y \bar{T}\}_v^2 > 0$, see Eq. 14).

Turbulent Surface Heat Flux Changes

Shaw et al. [53] used the MSE framework for storm tracks to show that the SH storm track intensifies in response to SST warming in prescribed SST AGCM simulations following the increase in the equator-to-pole energy gradient induced by changes in surface heat fluxes, i.e., more evaporation in the tropics than at the South Pole ($\Delta\langle v'm' \rangle = 2\pi a^2 \int_{\phi_s}^{-\pi/2} \cos\phi \Delta F_{SHF} d\phi > 0$, see Eq. 19).

Mechanisms Explaining the Weakening of the Zonal Mean Mid-Latitude Circulation

Here I review the mechanisms that have been proposed to explain the weakening of the zonal mean mid-latitude circulation in response to increased CO₂. Recall that a weakening of the zonal mean mid-latitude circulation occurs in response to increased CO₂ during NH summer. Most of the mechanisms below were not proposed to explain the seasonality of the NH response to increased CO₂. Thus, it is not clear in all cases why the mechanisms below should apply only during NH summer. It is possible that different mechanisms operate in NH winter and summer and that more than one mechanism operates in a given season. Once again, the mechanisms are grouped according to their thermodynamic starting point.

Increased Specific Humidity Following the Clausius-Clapeyron Relation

The following mechanisms rely on changes in specific humidity following the Clausius-Clapeyron relation:

- Held [23] argued that if the total MSE flux is constant in response to increased CO₂ ($\Delta\langle v'm' \rangle \approx 0$), then increased latent energy flux following the Clausius-Clapeyron relation ($\Delta\langle Lv'q' \rangle \approx \alpha \Delta T \langle Lv'q' \rangle < 0$ in the SH) should result in decreased DSE flux ($\Delta\langle v's' \rangle > 0$ in the SH), i.e., a weakening of the dry storm track.
 - Shaw and Voigt [52] showed that if one assumes the total MSE flux is constant in response to SST warming ($\Delta\langle v'm' \rangle \approx 0$) and the near-surface MSE gradient response to increased CO₂ follows the Clausius-Clapeyron relation ($\partial\Delta\bar{m}/\partial y \approx \alpha^2 \Delta T Lq \partial\bar{T}/\partial\phi/a < 0$), then the eddy diffusivity decreases [$\Delta D_m \approx -D_m (\alpha^2 \Delta T Lq \partial\bar{T}/\partial\phi/a)/(\partial\bar{m}/\partial y) < 0$, see Eq. 17 with $\Delta\langle v'm' \rangle \approx 0$ and $\partial\Delta\bar{m}/\partial y \approx \alpha^2 \Delta T Lq \partial\bar{T}/\partial\phi/a < 0$], i.e., the storm track weakens (see their Eq. 11) in aquaplanet models.
3. Radiative cooling of the stratosphere
 4. Hadley cell expansion
 5. Increased specific humidity following the Clausius-Clapeyron relation
 6. Cloud radiative effect changes
 7. Turbulent surface heat flux changes
 8. Decreased surface meridional temperature gradient

that have been proposed to explain the zonal mean mid-latitude circulation response to increased CO₂. While the mechanisms are not necessarily distinct, it is very unlikely that so many are needed to explain the response of the zonal mean mid-latitude circulation to increased CO₂. Since there are fewer thermodynamic starting points than mechanisms, it is useful to test the thermodynamic starting points. If a thermodynamic starting point is falsified, then all the mechanisms tied to it are falsified. If a thermodynamic starting point is confirmed, then more work is needed to determine which mechanism tied to that starting point is correct.

To date, there exist several different tests of thermodynamic starting points explaining the zonal mean mid-latitude circulation response to increased CO₂: (1) prescribing diabatic perturbations, (2) quantifying the transient response to an abrupt CO₂ increase, and (3) imposing latitudinally dependent CO₂ concentration. In what follows, I review how these approaches have been used to test whether the increased latent heat release aloft in the tropics starting point (see section “[Increased Latent Heat Release Aloft in the Tropics](#)”), hereafter referred to as the tropical starting point, can explain the annual mean poleward shift of the zonal mean mid-latitude circulation response to increased CO₂ in the SH.

For the prescribed diabatic perturbation approach, the test of the tropical starting point is conducted by prescribing a diabatic perturbation in the tropical upper troposphere, which mimics the tropical temperature response in CMIP5 models (Fig. 1, top), in a dry dynamical core model. If there is no poleward shift then the tropical starting point is falsified. The results of these tests show (1) raising the tropopause equatorward of the climatological jet shifts the jet equatorward [32] and (2) prescribing diabatic heating in the tropical upper troposphere leads to a poleward shift of the mid-latitude circulation only if the heating extends into the subtropics [4, 36, 59, 61].

It is difficult to interpret the results of tests that prescribe diabatic perturbations (e.g., prescribing diabatic heating in dry dynamical core simulations or prescribing the cloud radiative response to increased CO₂ in aquaplanet simulations) for several reasons. Prescribed diabatic perturbations require knowledge of the equilibrium response to increased CO₂, which is shaped by the circulation. The perturbations, including their meridional and vertical extent, have not been shown to occur in the absence of the circulation response, i.e., in radiative-convective equilibrium either without [60]

Increased Dry Static Stability Outside the Tropics

O’Gorman [47] showed the weakening of the zonal mean mid-latitude EKE during NH summer in response to increased CO₂ follows the decrease in MAPE, which is partly related to increased dry static stability ($\Delta\text{MAPE} \approx \frac{c_p p_0}{24g} (\sigma_s - \sigma_t^{\max}) L_Z^2 \Delta[\Gamma]_v [\{\partial_y \bar{T}\}]_v^2 < 0$, see Eq. 14).

Decreased Surface Meridional Temperature Gradient

In addition to the stability changes discussed above, Gertler and O’Gorman [16] showed that the weakening of the surface meridional temperature gradient in mid-latitudes around NH land also contributes to the decrease of nonconvective MAPE ($\Delta\text{MAPE} \approx \frac{c_p p_0}{24g} (\sigma_s - \sigma_t^{\max}) L_Z^2 [\Gamma]_v \Delta[\{\partial_y \bar{T}\}]_v^2 < 0$, see Eq. 14).

Turbulent Surface Heat Flux Changes

Shaw et al. [53] used the MSE framework for storm tracks to show that the storm track weakens in response to increased CO₂ over land during NH summer following the decreased equator-to-pole energy gradient induced by changes in surface heat fluxes over land, i.e., land warms more than the atmosphere and ocean ($\Delta\langle v'm' \rangle = \int_{\phi_s}^{-\pi/2} a \cos \phi \Delta F_{\text{SHF}} d\phi < 0$, see Eq. 19).

Testing Mechanisms

There are 24 mechanisms and 8 thermodynamic starting points:

1. Increased latent heat release aloft in the tropics
2. Increased dry static stability and tropopause height outside the tropics

or with the climatological circulation. Thus, it is possible the meridional extension of the prescribed diabatic heating into the subtropics is shaped by the circulation and encodes the circulation response. In order for tests involving prescribed diabatic perturbations to be useful the perturbations must be shown to occur in response to increased CO₂ in radiative-convective equilibrium either without [60] or with the climatological circulation.

The remaining approaches for testing the tropical starting point (quantifying the transient response to an abrupt CO₂ increase and imposing latitudinally dependent CO₂ concentration) do not suffer from the issues associated with prescribing diabatic perturbations because the diabatic response emerges as part of the model solution. For the transient response approach, the test of the tropical starting point is conducted by quantifying the timescale of the response of the tropical starting point and the zonal mean mid-latitude circulation shift to an abrupt CO₂ increase. If the timescale of the tropical response and mid-latitude shift are different, then the tropical starting point is falsified. Recent tests of the transient response to abrupt 4 × CO₂ in the SH in CMIP5 models shows the eddy momentum flux and eddy-driven jet evolve on a faster timescale than

the maximum absolute value of the upper tropospheric meridional temperature gradient from 0 to 45° S and the subtropical jet strength (compare the orange and purple lines to the blue and pink lines in Fig. 3), which are connected to the tropical starting point [42]. Using similar CMIP5 experiments, Chemke and Polvani [9] showed the eddy momentum flux also responds faster than the surface meridional temperature gradient in the subtropics. The fast timescale response of the eddy momentum flux and eddy-driven jet to an abrupt CO₂ increase is similar to that of subtropical dry static stability and the Hadley cell edge (compare the orange and purple lines to the red line in Fig. 3). The slow timescale response of the subtropical jet and maximum absolute value of the meridional temperature gradient to an abrupt CO₂ increase follows the evolution of global mean surface temperature, which is dominated by tropical adjustment. Interestingly, the eddy-driven jet also exhibits a distinct evolution in response to uniform sea surface temperature warming compared to the subtropical jet [11].

Finally, for the latitudinally dependent CO₂ concentration approach, the test of the tropical starting point is conducted by increasing CO₂ concentration only in the

Fig. 3 Time series of Southern Hemispheric response to abrupt 4 × CO₂ in CMIP5 models for **a** the Hadley cell edge (red) and strength (yellow), the subtropical jet position (green) and strength (blue) and the eddy-driven jet position divided by 2 (purple), **b** the latitude of maximum absolute value of the eddy momentum flux (orange) compared to the Hadley cell edge (red) and eddy-driven jet position divided by 2 (purple), and **c** the subtropical jet strength (blue) compared to the maximum absolute value of the meridional temperature gradient (pink) between 0 and 45° S. For each plot, shading represents the 95% confidence interval of model spread. In **(b)** the subset of models from **(a)** that provided 6-hourly data are used. Adapted from [42]

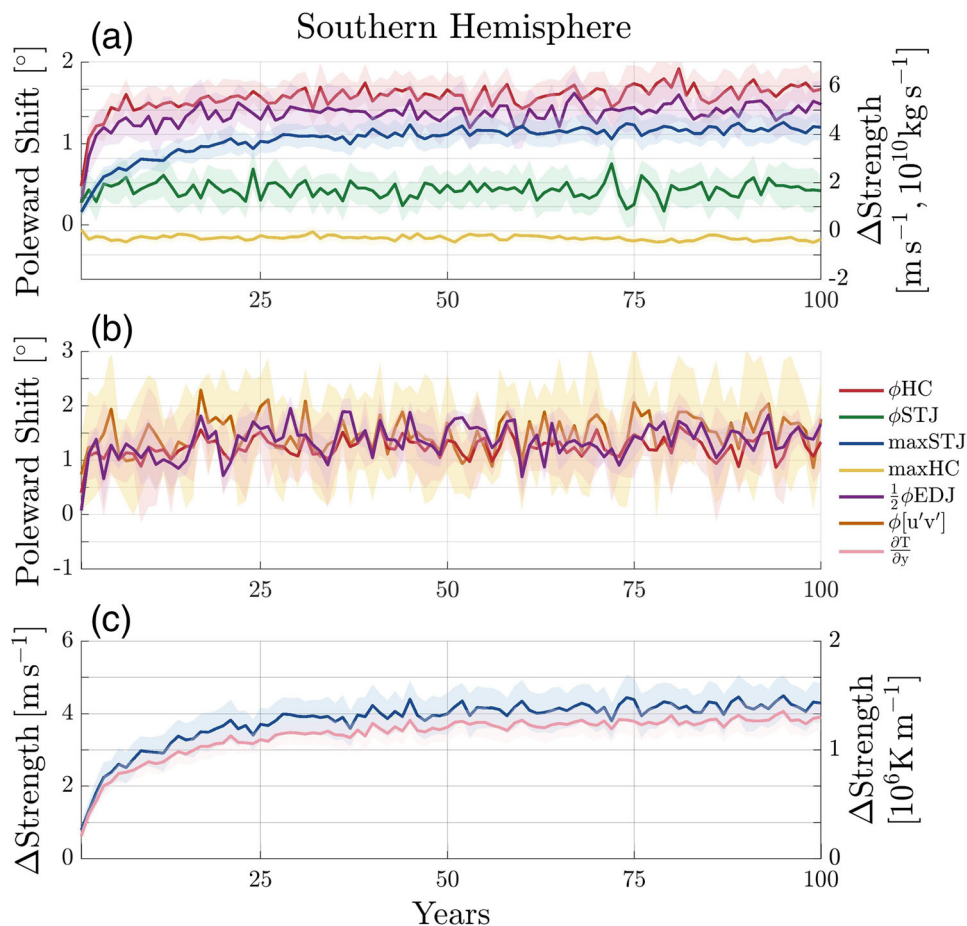
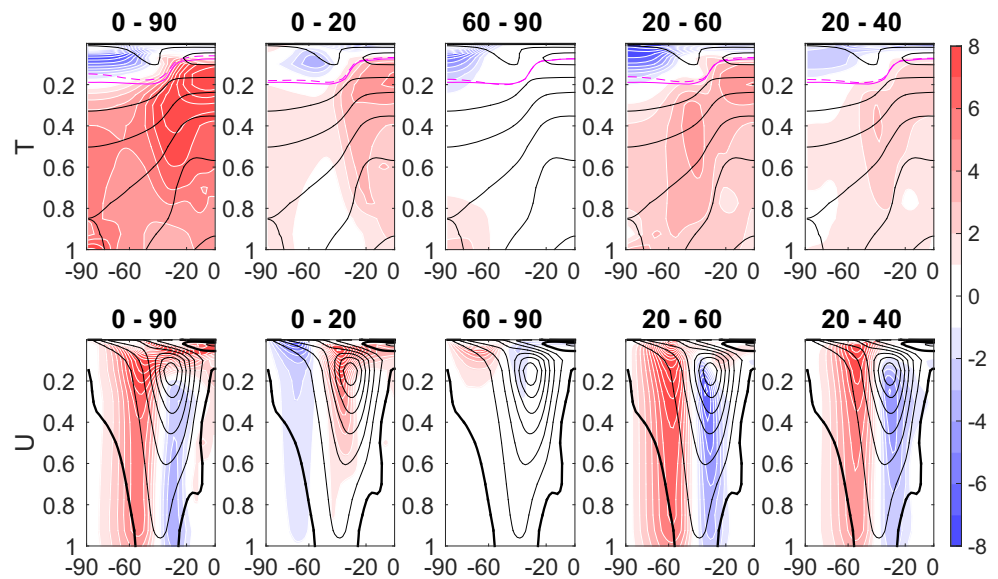


Fig. 4 As in Fig. 1 but for the ECHAM6 slab-ocean aquaplanet response to latitudinally dependent quadrupling of CO₂. Reproduced from [54]

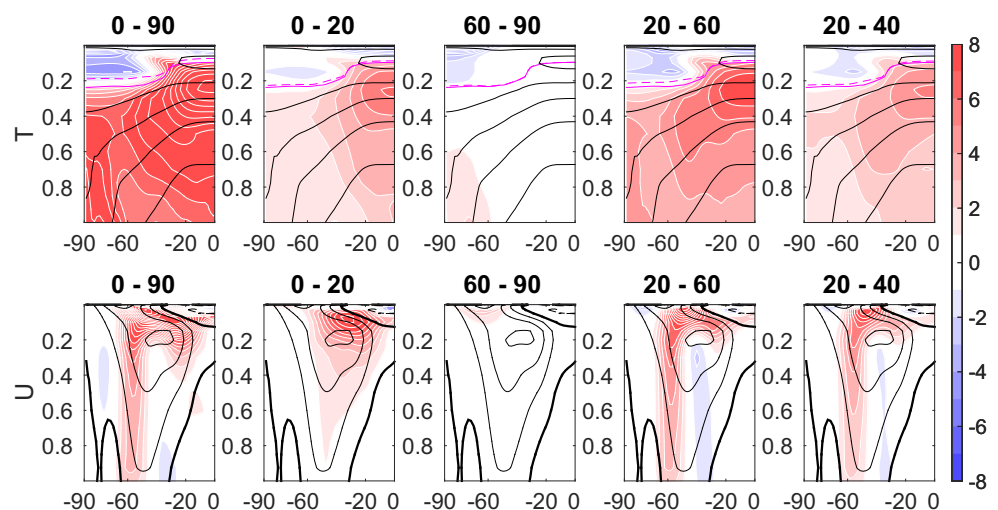


tropics (20° S to 20° N). The CO₂ concentration can be easily prescribed as a constant value in each latitudinal grid box for all longitudes in most climate models. If there is no poleward shift in response to the tropical CO₂ increase, then the tropical starting point is falsified, assuming the response to increased CO₂ is linear. The response is linear if the sum of the response to increased CO₂ in the tropics and outside the tropics is close to the response when CO₂ increases everywhere. Shaw and Tan [54] showed quadrupling CO₂ concentration in the tropics in aquaplanet models does not produce a significant circulation shift (Fig. 4) even though it does produce a large response of the subtropical meridional temperature gradient in the upper troposphere and subtropical jet strength. Similar results are obtained for the SH circulation when quadrupling CO₂ in the tropics of a slab-ocean AGCM with climatological q-flux (Fig. 5). The

SH response in the aquaplanet and AGCM are close to linear for a number of shift metrics (compare sum of red, blue, and green crosses to black cross in Fig. 6). The latitudinal decomposition shows quadrupling CO₂ in the subtropics dominates the poleward shift of the SH circulation in the aquaplanet and slab-ocean AGCM (Fig. 6).

Overall, the recent tests discussed above do not support the tropical starting point and its underlying mechanisms (see section “[Increased Latent Heat Release Aloft in the Tropics](#)”) as an explanation for the poleward shift of the SH mid-latitude circulation in response to increased CO₂. More specifically, (1) the meridional temperature gradient and subtropical jet strength evolve on a different timescale than the mid-latitude circulation shift in response to an abrupt CO₂ increase and (2) increased CO₂ in the tropics does not produce a significant poleward shift. Instead, the tests lend

Fig. 5 As in Fig. 1 but for the ECHAM6 slab-ocean AGCM response in the Southern Hemisphere to latitudinally dependent quadrupling of CO₂



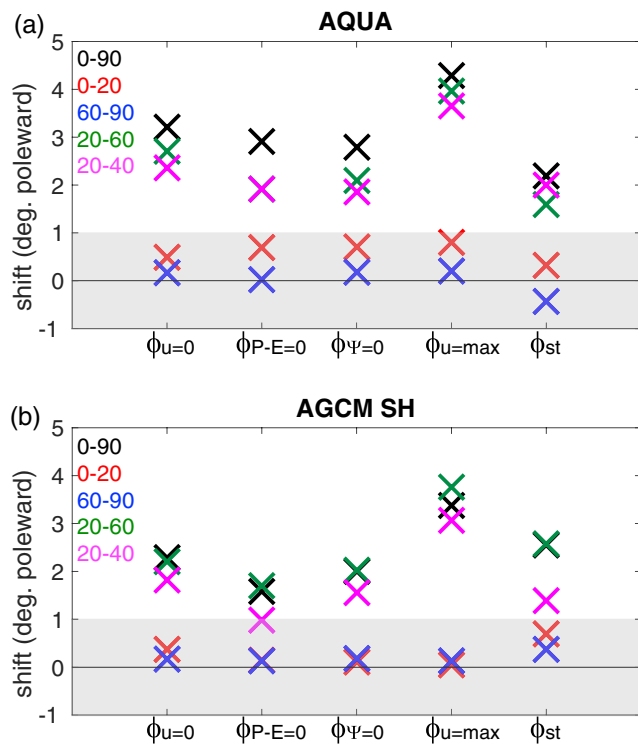


Fig. 6 Shift of latitude where u at 10 m is zero in the subtropics ($\phi_{u=0}$), precipitation minus evaporation is zero in the subtropics ($\phi_{P-E=0}$), Eulerian streamfunction is zero at 700 hPa ($\phi_{\Psi=0}$), u at 10 m is maximum in mid-latitudes ($\phi_{u=max}$) and transient eddy MSE flux is maximum in mid-latitudes (ϕ_{st}) in response to latitudinally dependent quadrupling of CO₂. Gray shading indicates shifts whose absolute value is $\leq 1^\circ$. Panel (a) reproduced from [54]

support to the increased dry static stability and tropopause height outside the tropics starting point (see section “Increased Dry Static Stability and Tropopause Height Outside the Tropics”). However, more tests are needed, including with climate models across the model hierarchy, before falsifying the tropical starting point. The results above demonstrate the importance of using climate models in novel ways to test mechanisms.

Future Outlook

Future progress in understanding the zonal mean mid-latitude circulation response to increased CO₂ relies on (1) carefully designed climate model experiments that attempt to falsify the thermodynamic starting points and assumptions underlying the proposed mechanisms and (2) subsequently using the remaining mechanisms to create emergent constraints. Several approaches can be used to test mechanisms, for example, (1) imposing diabatic perturbations based on the response to increased CO₂ in radiative-convective equilibrium either in the absence [60]

or presence of the climatological circulation, (2) quantifying the transient evolution of the circulation response to an abrupt CO₂ increase [9, 11, 17, 36, 42, 67, 68], (3) imposing latitudinally dependent CO₂ concentration [54], (4) quantifying the seasonality of the mechanisms, and (5) nudging parameters to their climatological value, e.g., turning off wind induced surface heat exchange [43]. Emergent constraints (see [19]) are needed in order to quantify and compare the modeled mechanisms to those in the real atmosphere. Finally, in addition to recommending more be done to falsify existing mechanisms, I would also recommend any new mechanism proposed in the future should (1) be simple, (2) be able to predict the circulation response without running a model, (3) involve an equation (to ensure transparency), and (4) be falsifiable.

Acknowledgments TAS thanks the section editor Isla Simpson and two anonymous reviewers for their comments and Molly Menzel for providing Fig. 3.

Compliance with Ethical Standards

Conflict of Interest The authors declare that they have no conflict of interest.

Funding Information TAS acknowledges support from the National Science Foundation (AGS-1742944) and the David and Lucile Packard Foundation.

Open Access This article is distributed under the terms of the Creative Commons Attribution 4.0 International License (<http://creativecommons.org/licenses/by/4.0/>), which permits unrestricted use, distribution, and reproduction in any medium, provided you give appropriate credit to the original author(s) and the source, provide a link to the Creative Commons license, and indicate if changes were made.

References

1. Barnes EA, Polvani LM. Response of the midlatitude jets, and of their variability, to increased greenhouse gases in the CMIP5 models. *J Clim*. 2013;26:7117–7135.
2. Barpanda P, Shaw T. Using the moist static energy budget to understand storm-track shifts across a range of time scales. *J Atmos Sci*. 2017;74:2427–2446.
3. Bender FA-M, Ramanathan V, Tselioudis G. Changes in extratropical storm track cloudiness 1983–2008: observational support for a poleward shift. *Clim Dyn*. 2012;28:2037–2053.
4. Butler AH, Thompson DWJ, Heikes R. The steady-state atmospheric circulation response to climate change-like thermal forcings in a simple general circulation Model. *J Clim*. 2010;23:3474–3496.
5. Butler AH, Thompson DWJ, Birner T. Isentropic slopes, downgradient eddy fluxes, and the extratropical atmospheric circulation response to tropical tropospheric heating. *J Atmos Sci*. 2011;68:2292–2305.
6. Ceppi P, Hartmann DL. Connections between clouds, radiation, and midlatitude dynamics: a review. *Curr Clim Chang Rep*. 2015;1:94–102.
7. Ceppi P, Hartmann DL. Clouds and the atmospheric circulation response to warming. *J Clim*. 2016;29:783–799.

8. Chang EKM, Guo Y, Xia X. CMIP5 multi-model ensemble projection of storm track change under global warming. *J Geophys Res.* <https://doi.org/10.1029/2012JD018578>. 2012.
9. Chemke R, Polvani LM. Exploiting the abrupt 4xCO₂ scenario to elucidate tropical expansion mechanisms. *J Clim.* 2019;32:859–875.
10. Chen G, Lu J, Frierson DMW. Phase speed spectra and the latitude of surface westerlies: interannual variability and global warming trend. *J Clim.* 2008;21:5942–5959.
11. Chen G, Lu J, Sun L. Delineating the eddy-zonal flow interaction in the atmospheric circulation response to climate forcing: uniform SST warming in an idealized aquaplanet model. *J Atmos Sci.* 2013;70:2214–2233.
12. Coumou D, Lehmann J, Beckmann J. The weakening summer circulation in the Northern Hemisphere mid-latitudes. *Science.* 2015;348:324–327.
13. Cronin TW, Jansen MF. Analytic radiative-advective equilibrium as a model for high-latitude climate. *Geophys. Res. Lett.* <https://doi.org/10.1002/2015GL067172>. 2016.
14. Frierson DMW. Midlatitude static stability in simple and comprehensive general circulation models. *J Atmos Sci.* 2008;65:1049–1062.
15. Fu Q, Johanson CM, Wallace JM, Reichler T. Enhanced mid-latitude tropospheric warming in satellite measurements. *Science.* 2006;312:1179.
16. Gertler CG, O’Gorman PA. Changing available energy for extratropical cyclones and associated convection in Northern Hemisphere summer. *Proc. Nat. Acad. Sciences.* <https://doi.org/10.1073/pnas.1812312116>. 2019.
17. Grise K, Polvani LM. Understanding the time scales of the tropospheric circulation response to abrupt CO₂ forcing in the Southern Hemisphere: Seasonality and the role of the stratosphere. *J Clim.* 2017;30:8497–8515.
18. Hall NJ, Hoskins BJ, Valdes PJ, Senior CA. Storm tracks in a high-resolution GCM with doubled carbon dioxide. *Quart J Roy Met Soc.* 1994;120:1209–1230.
19. Hall A, Cox P, Huntingford C, Klein S. Progressing emergent constraints on future climate change. *Nat Clim Chang.* 2019;9:269–278.
20. Held IM. Large-scale dynamics and global warming. *Bull Amer Met Soc.* 1993;74:228–241.
21. Held IM. The gap between simulation and understanding in climate modeling. *Bull. Amer. Met. Soc.* <https://doi.org/10.1175/BAMS-86-11-1609>. 2005.
22. Held IM, Soden BJ. Robust responses of the hydrological cycle to global warming. *J Clim.* 2006;19:5686–5699.
23. Held IM. Poleward atmospheric energy transport. <https://www.gfdl.noaa.gov/blog/held/62-poleward-atmospheric-energy-transport>. 2015.
24. Karoly DJ, Hoskins BJ. Three-dimensional propagation of planetary waves. *J Met Soc Jpn.* 1982;60:109–123.
25. Kidston J, Dean SM, Renwick JA, Vallis GK. A robust increase in the eddy length scale in the simulation of future climates. *Geophys. Res. Lett.* <https://doi.org/10.1029/2009GL041615>. 2010.
26. Kidston J, Vallis GK, Dean SM, Renwick JA. Can the increase in the eddy length scale under global warming cause the poleward shift of the jet streams. *J Clim.* <https://doi.org/10.1175/2010JCLI3738.1>. 2011.
27. Kidston J, Vallis GK. The relationship between the speed and the latitude of an eddy-driven jet in a stirred barotropic model. *J Atmos Sci.* <https://doi.org/10.1175/JAS-D-11-0300.1>. 2012.
28. Kuo H-L. Forced and free meridional circulations in the atmosphere. *J Meteorol.* 1956;13:561–568.
29. Kushner PJ, Held IM. A test, using atmospheric data of a method for estimating oceanic eddy diffusivity. *Geophys Res Lett.* 1998;25:4213–4216.
30. Lee S, Feldstein SB. Detecting ozone- and greenhouse gas-driven wind trends with observational data. *Science.* <https://doi.org/10.1126/science.1225154>. 2013.
31. Li Y, Thompson DWJ, Bony S, Merlis TM. Thermodynamic control on the poleward shift of the extratropical jet in climate change simulations: the role of rising high clouds and their radiative effects. *J Clim.* 2018;32:917–934.
32. Lorenz DJ, DeWeaver ET. Tropopause height and zonal wind response to global warming in the IPCC scenario integrations. *J Geophys Res.* <https://doi.org/10.1029/2006JD008087>. 2007.
33. Lorenz DJ. Understanding midlatitude jet variability and change using rossby wave chromatography: poleward-shifted jets in response to external forcing. *J Atmos Sci.* 2014;71:2370–2389.
34. Lu J, Vecchi GA, Reichler T. Expansion of the Hadley cell under global warming. *Geophys. Res Lett.* <https://doi.org/10.1029/2006GL028443>. 2007.
35. Lu J, Chen G, Frierson DMW. Response of the zonal mean atmospheric circulation to El Niño versus global warming. *J Clim.* 2008;21:5835–5851.
36. Lu J, Sun L, Wu Y, Chen G. The role of subtropical irreversible PV mixing in the zonal mean circulation response to global warming-like thermal forcing. *J Clim.* 2014;27:2297–2316.
37. Manabe S, Wetherald RT. The effects of doubling CO₂ concentration in a general circulation model. *J Atmos Sci.* 1975;32:3–15.
38. Matsuno T. Vertical propagation of stationary planetary waves in winter Northern Hemisphere. *J Atmos Sci.* 1970;27:871–883.
39. Mbengue C, Schneider T. Storm track shifts under climate change: what can be learned from large-scale dry dynamics. *J Clim.* 2013;26:9923–9930.
40. Mbengue C, Schneider T. Storm-track shifts under climate change: toward a mechanistic understanding using baroclinic mean available potential energy. *J Atmos Sci.* 2017;74:93–110.
41. Mbengue C, Schneider T. Linking Hadley circulation and storm tracks in a conceptual model of the atmospheric energy balance. *J Atmos Sci.* 2018;75:841–856.
42. Menzel ME, Waugh D, Grise K. Disconnect between Hadley cell and subtropical jet variability and response to increased CO₂. *Geophys. Res Lett.* <https://doi.org/10.1029/2019GL083345>. 2019.
43. Muller CJ, Romps DM. Acceleration of tropical cyclogenesis by self-aggregation feedbacks. *Proc Nat Acad Sci.* 2018;115:2930–2935.
44. Nakamura N, Zhu D. Finite-amplitude wave activity and diffusive flux of potential vorticity in eddy-mean flow interaction. *J Atmos Sci.* 2010;67:2701–2716.
45. Nakamura N, Solomon A. Finite-amplitude wave activity and mean flow adjustments in the atmospheric general circulation. Part I: quasigeostrophic theory and analysis. *J Atmos Sci.* 2010;67:3967–3983.
46. O’Gorman PA, Schneider T. Energy of midlatitude transient eddies in idealized simulations of changed climates. *J Clim.* 2008;21:5797–5806.
47. O’Gorman PA. Understanding the varied response of the extratropical storm tracks to climate change. *Proc Nat Acad Sci.* 2010;107:19176–19180.
48. Pfeffer RL. Wave-mean flow interactions in the atmosphere. *J Atmos Sci.* 1981;38:1340–1359.
49. Riviere G. A dynamical interpretation of the poleward shift of the jet streams in global warming scenarios. *J Atmos Sci.* 2011;68:1253–1272.
50. Schneider T. The general circulation of the atmosphere. *Annu. Rev. Earth Planet. Sci.* <https://doi.org/10.1146/annurev.earth.34.031405.125144>. 2006.
51. Shaw T, Baldwin M, Barnes EA, Caballero R, Garfinkel CI, Hwang Y-T, Li C, O’Gorman PA, Riviere G, Simpson I, Voigt

- A. Storm track processes and the opposing influences of climate change. *Nature Geoscience*. <https://doi.org/10.1038/NGEO2783>. 2016.
52. Shaw T, Voigt A. What can moist thermodynamics tell us about circulation shifts in response to uniform warming? *Geophys. Res Lett*. <https://doi.org/10.1002/2016GL068712>. 2016.
 53. Shaw T, Barpanda P, Donohoe A. A moist static energy framework for zonal-mean storm-track intensity. *J Atmos Sci*. 2018;75:1979–1994.
 54. Shaw T, Tan Z. Testing latitudinally dependent explanations of the circulation response to increased CO₂ using aquaplanet models. *Geophys. Res Lett*. <https://doi.org/10.1029/2018GL078974>. 2018.
 55. Sigmond M, Siegmund PC, Manzini E, Kelder H. A simulation of the separate climate effects of middle-atmospheric and tropospheric CO₂ doubling. *J Clim*. 2004;17:2352–2367.
 56. Simpson I, Shaw T, Seager R. A diagnosis of the seasonally and longitudinally varying midlatitude circulation response to global warming. *J Atmos Sci*. 2014;71:2489–2515.
 57. Staten PW, Lu J, Grise K, Davis SM, Birner T. Re-examining tropical expansion. *Nat Clim Chang*. 2018;8:768–775.
 58. Stevens B, Giorgetta M, Esch M, Mauritsen T, Cruieger T, Rast S, et al. Atmospheric component of the MPI-M earth system model: ECHAM6. *J. Adv. Mod. Earth Sys*. <https://doi.org/10.1002/jame.20015>. 2013.
 59. Sun L, Chen G, Lu J. Sensitivities and mechanisms of the zonal mean atmospheric circulation response to tropical warming. *J Atmos Sci*. 2013;70:2487–2504.
 60. Tan Z, Lachmy O, Shaw T. The sensitivity of the jet stream response to climate change to radiative assumptions. *J Adv Model Earth Sys*. 2019;11:1–23.
 61. Tandon N, Gerber EP, Sobel AH, Polvani LM. Understanding hadley cell expansion versus contraction: Insights from simplified models and implications for recent observations. *J Clim*. 2013;26:4304–4321.
 62. Trenberth KE, Stepaniak DP. Covariability of components of poleward atmospheric energy transports on seasonal and interannual timescales. *J Clim*. 2003;16:3691–3705.
 63. Vallis GK. *Atmospheric and oceanic fluid dynamics*. Cambridge: Cambridge University Press; 2006.
 64. Vallis GK, Zurita-Gotor P, Cairns C, Kidston J. Response of the large-scale structure of the atmosphere to global warming. *Quart J Roy Met Soc*. 2015;141:1479–1501.
 65. Voigt A, Shaw T. Circulation response to warming shaped by radiative changes of clouds and water vapour. *Nature Geoscience*. <https://doi.org/10.1038/NGEO2345>. 2015.
 66. Voigt A, Shaw T. Impact of regional atmospheric cloud radiative changes on shifts of the extratropical jet stream in response to global warming. *J Clim*. 2016;29:8399–8421.
 67. Wu Y, Seager R, Ting M, Naik N, Shaw T. Circulation response to an instantaneous doubling of carbon dioxide. Part I: model experiments and transient thermal response in the troposphere. *J Clim*. 2012;25:2862–2879.
 68. Wu Y, Seager R, Shaw T, Ting M, Naik N. Atmospheric circulation response to an instantaneous doubling of carbon dioxide. part II: atmospheric transient adjustment and its dynamics. *J Clim*. 2013;26:918–935.
 69. Yin JH. A consistent poleward shift of the storm tracks in simulations of 21st century climate. *Geophys. Res Lett*. <https://doi.org/10.1029/2005GL023684>. 2005.

Publisher's Note Springer Nature remains neutral with regard to jurisdictional claims in published maps and institutional affiliations.